

“Colloid–Atom Duality” in the Assembly Dynamics of Concave Gold Nanoarrows

Chang Liu, Zihao Ou, Fucheng Guo, Binbin Luo, Wenxiang Chen, Limin Qi,* and Qian Chen*



Cite This: <https://dx.doi.org/10.1021/jacs.0c04444>



Read Online

ACCESS |



Metrics & More



Article Recommendations



Supporting Information

ABSTRACT: We use liquid-phase transmission electron microscopy (TEM) to study self-assembly dynamics of charged gold nanoarrows (GNAs), which reveal an unexpected “colloid–atom duality”. On one hand, they assemble following the Derjaguin–Landau–Verwey–Overbeek (DLVO) theory for *colloids* when van der Waals attraction overruns slightly screened electrostatic repulsion. Due to concaveness in shape, GNAs adopt zipper motifs with lateral offset in their assembly matching with our modeling of inter-GNA interaction, which form into unconventional structures resembling degenerate crystals. On the other hand, further screening of electrostatic repulsion leads to merging of clusters assembled from GNAs, reminiscent of the coalescence growth mode in *atomic* crystals driven by minimization of surface energy, as we measure from the surface fluctuation of clusters. Liquid-phase TEM captures the initial formation of highly curved necks bridging the two clusters. Analysis of the real-time evolution of neck width illustrates the first-time observation of coalescence in colloidal assemblies facilitated by rapid surface diffusion of GNAs. We attribute the duality to the confluence of factors (e.g., nanoscale colloidal interaction, diffusional dynamics) that we access by liquid-phase TEM, taking turns to dominate at different conditions, which is potentially generic to the nanoscale. The atom aspect, in particular, can inspire utilization of atomic crystal synthesis strategies to encode structure and dynamics in nanoscale assembly.

Micron-sized colloids have been historically related to atoms as the minimal “visible” model atoms since the first direct imaging of their phase transition dynamics by optical microscopy in 2001.¹ Yet there exists a difference of 3 to 4 orders of magnitude in the size of colloids and atoms, which accounts for fundamental inconsistencies in their phase behaviors. For example, the prevalent assembly mechanisms for atoms such as coalescence² and oriented attachment³ have not been retrieved in micron-sized colloids at equilibrium.^{4–7} Contributing factors can be either the short-range nature of interactions between micron-sized colloids, which leads to a more corrugated energy landscape than that of atoms,⁵ or slower diffusion of micron-sized colloids,^{4,6} both making micron-sized colloids more prone to kinetic traps and not sampling their energy landscape sufficiently. The intermediate nanoscale can bridge the length scales but has been underexplored due to the lack of a counterpart of optical microscopy, capable of monitoring and tracking the motions of single nanosized entities.^{5,8–13} Conventional ensemble spectroscopy characterization of solutions^{8–10} and transmission electron microscopy (TEM) imaging of dry samples^{11–13} do not give single-particle-level dynamics. Liquid-phase TEM, which makes the nanometer resolution of TEM compatible with solutions, has frequent complications from illuminated substrate^{14–16} and sluggish nanoparticle motions,^{17,18} limiting its capability to retrieve bulk phase behaviors.

Here we fill the gap using our recently optimized low-dose liquid-phase TEM to reveal the self-assembly dynamics of gold nanoarrows (GNAs), which show a remarkable “colloid–atom duality”. The GNAs are synthesized following our previous method¹⁹ (Figure 1a, Figure S1a–b, Supporting Information), exhibiting a double-headed arrow shape (128.9 ± 8.5 nm in length L and 54.2 ± 3.1 nm in head width W , Figure S1c), with

two pyramidal heads connected by a four-wing shaft made of four panels radiating from the central shaft. The TEM images of the GNAs show that each wing has a thickness t_{GNA} of 10.1 ± 1.2 nm and a length l of 52.3 ± 7.8 nm, with a concave angle α of $83.7^\circ \pm 2.7^\circ$ (Figure 1a, Figure S1b–c). GNAs are coated with carboxylated thiols, negatively charged in pH-neutral water or basic buffer (Figure S1d). Low dose rates ($7.4\text{--}12.9$ e[−] Å^{−2} s^{−1}) are used in imaging, which keep the ligands intact and induce controllable change in interparticle interactions.^{20,21} Different from the convex-shaped nanoparticles prevalently studied using this tool (e.g., spheres,^{16,22–28} rods,^{29,30} prisms^{20,21,31}), GNAs have geometric concaveness, endowing them with more complexity and tunability in balancing colloidal interaction¹⁹ with diffusion dynamics to achieve the duality. The resultant diversity in the assemblies can potentially introduce dynamic optical properties, such as structure-dependent optical absorption³² and polarization control,³³ which are important for the design of optical absorbers³² and active metamaterials.^{33,34}

The *colloidal* aspect of assembly dynamics occurs at ionic strength $I = 6.4$ mM, where van der Waals attraction between GNAs dominates a screened electrostatic repulsion, leading to dynamically reorganizing assemblies consisting of a “zipper” motif. As shown in Movie S1, the GNAs locally concentrate and assemble side-by-side, with centroids labeled to map inter-GNA

Received: April 22, 2020

Published: June 16, 2020



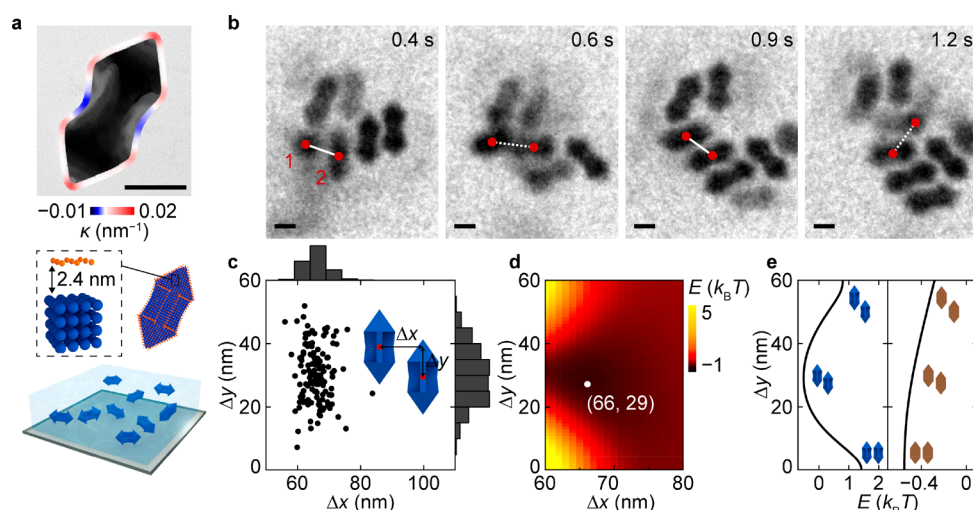


Figure 1. Colloidal aspect of the duality of GNAs assembling following the zipper motif. (a) Top: TEM image of GNA with the outline colored to local curvature κ . Bottom: 3D discretized model of a GNA with gold atoms (blue) and surface charges (orange), and schematic of SiN_x liquid chamber. (b) Time-lapse liquid-phase TEM images of GNAs assembling at $I = 6.4$ mM. The labeled GNA pair is dynamically connected (solid line) and disconnected (dash line). Dose rate: $7.4 \text{ e}^- \text{ \AA}^{-2} \text{ s}^{-1}$. (c) Histogram of the configuration of a connected GNA pair analyzed from [Movie S1](#) and [Movie S2](#). Inset schematic defines Δx and Δy . (d) The calculated E as a function of Δx and Δy defined in (c). White filled circle denotes energy minimum. (e) The calculated E for the GNA pair (blue) and hypothetical f -GNA pair as a reference (brown) at fixed Δx of the energy minimum (66 and 84 nm, respectively) and varying Δy . Scale bars: 50 nm.

connections ([Figure 1b](#)). The position, orientation, and connection of the GNAs undergo rapid rearrangements at a time interval as small as 0.2 s. The tracked nearest neighboring distances $r_{\text{n.n.}}$ of all the GNAs in the view average at a finite length of 82.8 nm ([Figure S2a–b](#)), confirming net inter-GNA attraction despite fast shuffling of GNAs. As an example, the distance between GNAs 1 and 2 (labeled in [Figure 1b](#)) fluctuates between 80.3 and 91.5 nm ([Figure S2c](#)), suggesting dynamic reorganization, differing from irreversible aggregation in previous liquid-phase TEM studies.^{16,21,29,30} Statistical tracking of the configurations of a connected GNA pair shows single-peaked distribution of the Δx spacing (averaged at 65.9 nm, defined as the distance between the centroid of one GNA and the long axis of the other GNA) and the Δy offset (averaged at 30.1 nm) along the long axis of parallel GNAs ([Figure 1c](#)), favoring the “zipper” motif.

Our interaction modeling elucidates the key role of local concaveness generic to the GNA shape in favoring the dynamic “zipper” motif. Using a three-dimensional (3D) discretized model built on the measured shape descriptors ([Figure S1b–c](#)), we compute the pairwise interparticle interaction E from the interparticle van der Waals attraction (E_{vdW}) and electrostatic repulsion (E_{el}) ($E = E_{\text{vdW}} + E_{\text{el}}$ following DLVO theory³⁵) as a function of different pairing configurations. As shown in [Figure 1d](#), E has a minimum at $\Delta x = 66$ nm and $\Delta y = 29$ nm, matching with the zipper motif. The weak attraction strength ($-0.5k_{\text{B}}T$) suggests thermal fluctuations are sufficient to overcome the net inter-GNA attraction, consistent with our experimental observation of dynamic assemblies. The concaveness accounts for the misalignment, consistent with previous studies^{36,37} illustrating the role of surface curvature in dictating assembly; conversely, when we consider hypothetical flat GNAs (f -GNAs, [Figure S1c](#)) with a cuboidal body (no concaveness) while keeping all the other features the same, the minimum of E occurs at $\Delta y = 0$ nm with no offset ([Figure 1e](#)).

The zipper motif is essential to further assemble into unexpected structures resembling degenerate crystal (DC).³⁸ The three preferred alignments of the GNAs ([Figure 2a](#)) and

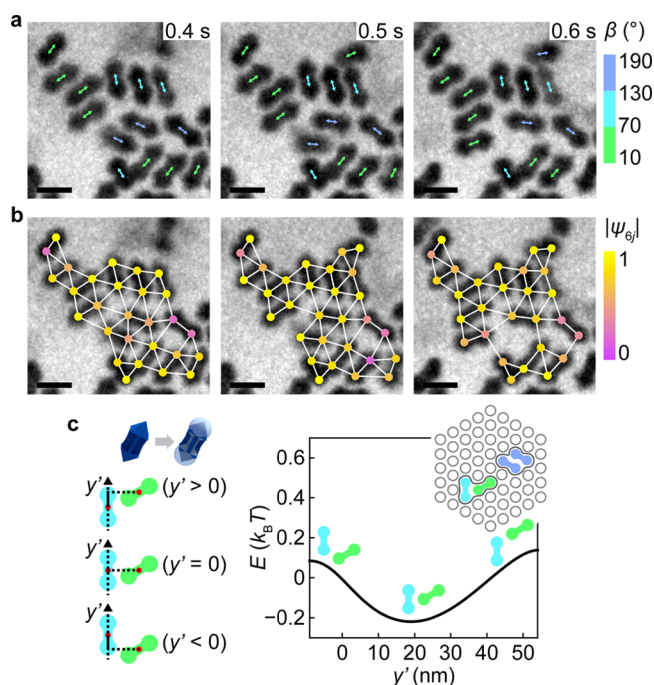


Figure 2. Assembly of GNAs into DC-like structures. (a) Time-lapse liquid-phase TEM images with the orientation β of GNAs marked. $I = 6.4$ mM; $7.4 \text{ e}^- \text{ \AA}^{-2} \text{ s}^{-1}$ ([Movie S2](#)). (b) The same TEM images as those in (a) with the lobe positions colored to $|\psi_{6j}|$ and the DC connections marked (white lines). (c) Left: Definition of y' as the coordinate of the right GNA when setting the left GNA as the vertical axis. The GNA is simplified as two lobes connected by a rod. Right: The calculated E of a GNA pair at fixed $\Delta\beta = 60^\circ$ and $\Delta x = 94.2$ nm, with varying y' . Inset: Two pairing motifs (zipper and boomerang) of GNAs. Scale bars: 100 nm.

triangular ordering (see the labeled GNA lobes in [Figure 2b](#)) are typical of a DC structure, potentially allowing for polarization control of incident light.^{33,39} The 6-fold bonding symmetry of each lobe j measured using the modulus bond-orientational

order parameter⁴⁰ $|\psi_{6l}|$ shows a consistent high order spanning the whole structure (Figure 2b). This periodicity of DC structure can produce diffractive waves by GNAs scattering light, which can narrow plasmon resonances for applications in optoelectronics, photovoltaics, and biosensing.^{41,42} Besides the specific zipper motif favored at $I = 6.4$ mM (Figure S2d), another “boomerang” motif ($\Delta\beta = 60^\circ$, $\Delta x = 94.2$ nm, $y' = 18.1$ nm defined in Figure 2c) is also essential for the DC-like structure to form. Our calculated pairwise interaction E for a GNA pair at fixed $\Delta\beta$ and Δx (Figure 2c) reaches its minimum at $y' = 19$ nm, validating the enthalpic preference for the boomerang motif.

The concaveness in our GNAs allows for a wide range of interaction tunability: at $I = 120$ mM, GNAs are further screened electrostatically and exhibit a surprising coalescence growth analogous to that in atomic crystallization. Interaction modeling rationalizes that GNAs assemble into clusters of various motifs (Figure 3c). At low GNA concentration, the clusters are small

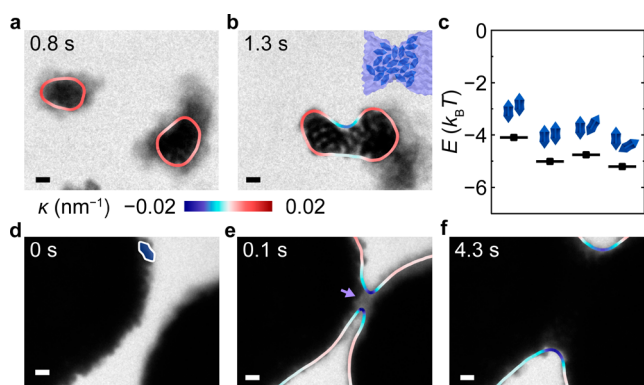


Figure 3. Atomic aspect of the duality: coalescence of clusters assembled from GNAs. Time-lapse liquid-phase TEM images showing the coalescence of two small clusters (a–b), and two large clusters (d–f). The boundaries of the clusters involved in coalescence are colored to κ . $12.9 \text{ e}^- \text{ \AA}^{-2} \text{ s}^{-1}$. Scale bars: 100 nm. (c) The calculated E for different GNA pair configurations at $I = 120$ mM.

(<30 GNAs), diffusing and rearranging quickly as a whole after coalescence (Movie S3, Figure 3a–b). In comparison, at high GNA concentration, the clusters are large (>100 GNAs) and diffuse slower than the small clusters,²² exhibiting the formation of a neck as some surface GNAs of the two clusters come into physical contact (Movie S4).

New surfaces are formed at the neck periphery of high curvature (Figure 3d–f). The neck’s apices are tracked over time t with the interapex distance measured as the neck width d_{neck} . In atomic crystallization, volume diffusion and surface diffusion of atoms are the dominant mass transport paths during coalescence. We measure a power law of $d_{\text{neck}} \sim t^{0.24}$ (Figure 4a), indicating surface diffusion ($d_{\text{neck}} \sim t^{0.16}$) as predicted by the classical continuum theory.^{43,44}

Coalescence is usually attributed to the minimization of the free energy by reducing surface area. Indeed, the upper contour of the coalescing neck (Figure 4b) shows a decrease in the high-curvature regions, while regions of low curvature remain (Figure 4c). The curvature–growth rate histogram (Figure 4d) shows a positive interrelation of these two factors, consistent with a curvature-dependent flattening effect to minimize surface area.⁴⁵ We measure the surface energy gain for coalescence following a capillary wave theory (CWT) (Supporting Information),⁴⁶ which describes how thermal fluctuation equilibrates with surface energy in defining the spatiotemporal fluctuation of a

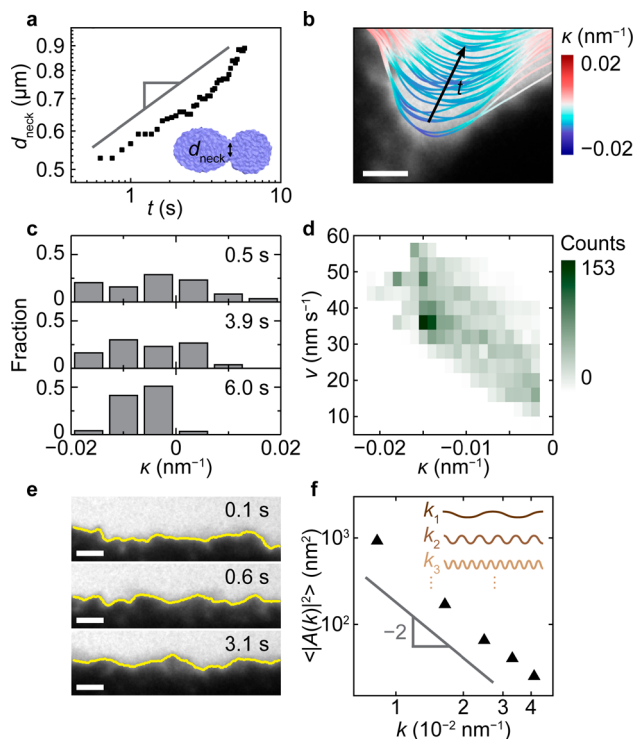


Figure 4. Neck evolution during coalescence. (a) Evolution of d_{neck} (black squares) with t . (b) Forty-eight time-lapse contours of the growing neck in Movie S4 (0.12 s time interval) overlaid with the starting TEM frame ($t = 0.2$ s). (c) Histogram of κ of the neck contours selected from (b), with statistics of two adjacent frames at 0.5 s, 3.9 s, and 6.0 s, respectively. (d) Local curvature (κ)–growth rate (ν) histogram (Movie S4), including only the ν values at neck regions of negative curvatures. (e) Time-lapse liquid-phase TEM images showing the fluctuating surface of the cluster composed of GNAs. (f) Dependences of $\langle |A(k)|^2 \rangle$ on k on a log–log scale plot. The gray line denotes a power law of -2 . Scale bars: 100 nm.

surface. Specifically, we track the regional surface profile of a cluster (Movie S5, Figure 4e), from which we derive a height function $h(x, t)$. The height function is then decomposed into a series of sinusoidal waves of wave vector k , based on which we verify that the squared time-averaged Fourier coefficient ($\langle |A(k)|^2 \rangle$) fits with $k^{-2.2}$ (Figure 4f), consistent with the prediction of CWT ($\langle |A(k)|^2 \rangle \sim k^{-2}$). This applicability of CWT allows us to calculate the surface energy as $(1.26 \pm 0.02) \times 10^{-13} \text{ J/m}$ (Figure S3). Note that our observation of the neck formed during coalescence starts from $d_{\text{neck}} = 104$ nm, corresponding to a surface energy gain of $3.2k_B T$, sufficient for coalescence to happen.

We attribute the observation of such coalescence behavior in GNAs to the faster diffusion of nanoparticles than that of micron-sized colloids, which makes it hard for micron-sized colloids to exhibit a similar collective mass transport. In fact, the diffusion dynamics can be regulated by particle–substrate interaction for solvent-evaporation-driven or templated assemblies. For example, Figures S4 and S5 show that the same GNAs can exhibit suppressed motions at a lower I , following Langmuir-like adsorption on the SiN_x membrane. The “colloid–atom duality” illustrated here suggests that modification of diffusional dynamics of nanoparticles could facilitate atom-resembling behaviors as an unexplored playground in nanoscale assembly, offering more routes toward diverse functional and reconfigurable structures.^{47,48}

■ ASSOCIATED CONTENT**SI Supporting Information**

The Supporting Information is available free of charge at <https://pubs.acs.org/doi/10.1021/jacs.0c04444>.

Materials and Methods, Image and Data Analysis, Interaction Modeling, Figures S1–S5, Supplementary Movie Legends, and Supplementary References (PDF)

Movie S1: Liquid-phase TEM movie showing the zipper motifs of GNAs assembled at $I = 6.4$ mM. Dose rate: $7.4 \text{ e}^- \text{ A}^{-2} \text{ s}^{-1}$. The movie is played at 8 fps, real time. Scale bar: 100 nm. (AVI)

Movie S2: Synchronized movie including liquid-phase TEM movies of the self-assembly of GNAs into 2D degenerate crystal-like structure marked with single GNA orientation β (top left) and the local modulus bond-orientational order parameter $|\psi_6|$ (top right), and the corresponding standard deviation of the histogram of GNA orientations and the ensemble averaged local structure order parameter $|\psi_6|$ vs time t at $I = 6.4$ mM. Dose rate: $7.4 \text{ e}^- \text{ A}^{-2} \text{ s}^{-1}$. The movie is played at 2 fps, 0.25 \times real time. Scale bars: 100 nm. (AVI)

Movie S3: Liquid-phase TEM movie showing the coalescence of two small clusters assembled from GNAs, at low GNA concentration at $I = 120$ mM. Dose rate: $12.9 \text{ e}^- \text{ A}^{-2} \text{ s}^{-1}$. The movie is played at 8 fps, real time. Scale bar: 100 nm. (AVI)

Movie S4: Liquid-phase TEM movie showing the coalescence of the two large clusters at a high GNA concentration at $I = 120$ mM. The contours are colored to the local curvature κ . Dose rate: $12.9 \text{ e}^- \text{ A}^{-2} \text{ s}^{-1}$. The movie is played at 8 fps, real time. Scale bar: 100 nm. (AVI)

Movie S5: Liquid-phase TEM movie showing the fluctuating surface (highlighted by yellow) of a cluster at a high GNA concentration at $I = 120$ mM. Dose rate: $12.9 \text{ e}^- \text{ A}^{-2} \text{ s}^{-1}$. The movie is played at 8 fps, real time. Scale bar: 100 nm. (AVI)

■ AUTHOR INFORMATION**Corresponding Authors**

Limin Qi – Beijing National Laboratory for Molecular Sciences, College of Chemistry, Peking University, Beijing 100871, China; orcid.org/0000-0003-4959-6928; Email: liminqi@pku.edu.cn

Qian Chen – Department of Materials Science and Engineering, Materials Research Laboratory, Beckman Institute for Advanced Science and Technology, and Department of Chemistry, University of Illinois at Urbana–Champaign, Urbana, Illinois 61801, United States; orcid.org/0000-0002-1968-441X; Email: qchen20@illinois.edu

Authors

Chang Liu – Department of Materials Science and Engineering, University of Illinois at Urbana–Champaign, Urbana, Illinois 61801, United States

Zihao Ou – Department of Materials Science and Engineering, University of Illinois at Urbana–Champaign, Urbana, Illinois 61801, United States; orcid.org/0000-0003-2987-7423

Fucheng Guo – Beijing National Laboratory for Molecular Sciences, College of Chemistry, Peking University, Beijing 100871, China

Binbin Luo – Department of Materials Science and Engineering, University of Illinois at Urbana–Champaign, Urbana, Illinois 61801, United States

Wenxiang Chen – Department of Materials Science and Engineering, University of Illinois at Urbana–Champaign, Urbana, Illinois 61801, United States; orcid.org/0000-0003-1022-9514

Complete contact information is available at: <https://pubs.acs.org/doi/10.1021/jacs.0c04444>

Notes

The authors declare no competing financial interest.

■ ACKNOWLEDGMENTS

This work was supported by the American Chemical Society Petroleum Research Fund PRF No. 58515-DNI10 (liquid-phase TEM imaging and data analysis) and National Natural Science Foundation of China (Grant No. 21673007) (GNA synthesis method development). We thank John W. Smith and Dr. Cong Xu at University of Illinois at Urbana–Champaign and Dr. Qian Wang at Peking University for useful discussions.

■ REFERENCES

- (1) Gasser, U.; Weeks, E. R.; Schofield, A.; Pusey, P. N.; Weitz, D. A. Real-space imaging of nucleation and growth in colloidal crystallization. *Science* **2001**, *292*, 258–262.
- (2) Yuk, J. M.; Park, J.; Ercius, P.; Kim, K.; Hellebusch, D. J.; Crommie, M. F.; Lee, J. Y.; Zettl, A.; Alivisatos, A. P. High-resolution EM of colloidal nanocrystal growth using graphene liquid cells. *Science* **2012**, *336*, 61–64.
- (3) Zhang, X.; He, Y.; Sushko, M. L.; Liu, J.; Luo, L.; De Yoreo, J. J.; Mao, S. X.; Wang, C.; Rosso, K. M. Direction-specific van der Waals attraction between rutile TiO₂ nanocrystals. *Science* **2017**, *356*, 434–437.
- (4) Ganapathy, R.; Buckley, M. R.; Gerbode, S. J.; Cohen, I. Direct measurements of island growth and step-edge barriers in colloidal epitaxy. *Science* **2010**, *327*, 445–448.
- (5) Kleppmann, N.; Schreiber, F.; Klapp, S. H. L. Limits of size scalability of diffusion and growth: Atoms versus molecules versus colloids. *Phys. Rev. E: Stat. Phys., Plasmas, Fluids, Relat. Interdiscip. Top.* **2017**, *95*, No. 020801.
- (6) Xie, R.; Liu, X.-Y. Controllable epitaxial crystallization and reversible oriented patterning of two-dimensional Colloidal Crystals. *J. Am. Chem. Soc.* **2009**, *131*, 4976–4982.
- (7) Silvera Batista, C. A.; Larson, R. G.; Kotov, N. A. Nonadditivity of nanoparticle interactions. *Science* **2015**, *350*, 1242477.
- (8) Jones, M. R.; Macfarlane, R. J.; Lee, B.; Zhang, J.; Young, K. L.; Senesi, A. J.; Mirkin, C. A. DNA-nanoparticle superlattices formed from anisotropic building blocks. *Nat. Mater.* **2010**, *9*, 913–917.
- (9) Macfarlane, R. J.; Lee, B.; Jones, M. R.; Harris, N.; Schatz, G. C.; Mirkin, C. A. Nanoparticle superlattice engineering with DNA. *Science* **2011**, *334*, 204–208.
- (10) Wu, L.; Willis, J. J.; McKay, I. S.; Diroll, B. T.; Qin, J.; Cargnello, M.; Tassone, C. J. High-temperature crystallization of nanocrystals into three-dimensional superlattices. *Nature* **2017**, *548*, 197–201.
- (11) Boles, M. A.; Engel, M.; Talapin, D. V. Self-assembly of colloidal nanocrystals: From intricate structures to functional materials. *Chem. Rev.* **2016**, *116*, 11220–11289.
- (12) Ye, X.; Chen, J.; Engel, M.; Millan, J. A.; Li, W.; Qi, L.; Xing, G.; Collins, J. E.; Kagan, C. R.; Li, J.; Glotzer, S. C.; Murray, C. B. Competition of shape and interaction patchiness for self-assembling nanoplates. *Nat. Chem.* **2013**, *5*, 466–473.
- (13) Ye, X.; Zheng, C.; Chen, J.; Gao, Y.; Murray, C. B. Using binary surfactant mixtures to simultaneously improve the dimensional tunability and monodispersity in the seeded growth of gold nanorods. *Nano Lett.* **2013**, *13*, 765–771.

- (14) Chee, S. W.; Anand, U.; Bisht, G.; Tan, S. F.; Mirsaidov, U. Direct observations of the rotation and translation of anisotropic nanoparticles adsorbed at a liquid–solid interface. *Nano Lett.* **2019**, *19*, 2871–2878.
- (15) Chee, S. W.; Baraissov, Z.; Loh, N. D.; Matsudaira, P. T.; Mirsaidov, U. Desorption-mediated motion of nanoparticles at the liquid–solid interface. *J. Phys. Chem. C* **2016**, *120*, 20462–20470.
- (16) Liu, Y.; Lin, X.-M.; Sun, Y.; Rajh, T. In situ visualization of self-assembly of charged gold nanoparticles. *J. Am. Chem. Soc.* **2013**, *135*, 3764–3767.
- (17) Verch, A.; Pfaff, M.; de Jonge, N. Exceptionally slow movement of gold nanoparticles at a solid/liquid interface investigated by scanning transmission electron microscopy. *Langmuir* **2015**, *31*, 6956–6964.
- (18) White, E. R.; Mecklenburg, M.; Shevitski, B.; Singer, S. B.; Regan, B. C. Charged nanoparticle dynamics in water induced by scanning transmission electron microscopy. *Langmuir* **2012**, *28*, 3695–3698.
- (19) Wang, Q.; Wang, Z.; Li, Z.; Xiao, J.; Shan, H.; Fang, Z.; Qi, L. Controlled growth and shape-directed self-assembly of gold nanoarrows. *Sci. Adv.* **2017**, *3*, No. e1701183.
- (20) Kim, J.; Jones, M. R.; Ou, Z.; Chen, Q. In situ electron microscopy imaging and quantitative structural modulation of nanoparticle superlattices. *ACS Nano* **2016**, *10*, 9801–9808.
- (21) Kim, J.; Ou, Z.; Jones, M. R.; Song, X.; Chen, Q. Imaging the polymerization of multivalent nanoparticles in solution. *Nat. Commun.* **2017**, *8*, 761.
- (22) Lee, J.; Nakouzi, E.; Song, M.; Wang, B.; Chun, J.; Li, D. Mechanistic understanding of the growth kinetics and dynamics of nanoparticle superlattices by coupling interparticle forces from real-time measurements. *ACS Nano* **2018**, *12*, 12778–12787.
- (23) Lin, G.; Chee, S. W.; Raj, S.; Král, P.; Mirsaidov, U. Linker-mediated self-assembly dynamics of charged nanoparticles. *ACS Nano* **2016**, *10*, 7443–7450.
- (24) Park, J.; Zheng, H.; Lee, W. C.; Geissler, P. L.; Rabani, E.; Alivisatos, A. P. Direct observation of nanoparticle superlattice formation by using liquid cell transmission electron microscopy. *ACS Nano* **2012**, *6*, 2078–2085.
- (25) Keskin, S.; Besztejan, S.; Kassier, G.; Manz, S.; Bücker, R.; Riekeberg, S.; Trieu, H. K.; Rentmeister, A.; Miller, R. J. D. Visualization of multimerization and self-assembly of DNA-functionalized gold nanoparticles using in-liquid transmission electron microscopy. *J. Phys. Chem. Lett.* **2015**, *6*, 4487–4492.
- (26) Anand, U.; Lu, J.; Loh, D.; Aabdin, Z.; Mirsaidov, U. Hydration layer-mediated pairwise interaction of nanoparticles. *Nano Lett.* **2016**, *16*, 786–790.
- (27) Powers, A. S.; Liao, H.-G.; Raja, S. N.; Bronstein, N. D.; Alivisatos, A. P.; Zheng, H. Tracking nanoparticle diffusion and interaction during self-assembly in a liquid cell. *Nano Lett.* **2017**, *17*, 15–20.
- (28) Lee, J.; Nakouzi, E.; Xiao, D.; Wu, Z.; Song, M.; Ophus, C.; Chun, J.; Li, D. Interplay between short- and long-ranged forces leading to the formation of Ag nanoparticle superlattice. *Small* **2019**, *15*, 1901966.
- (29) Chen, Q.; Cho, H.; Manthiram, K.; Yoshida, M.; Ye, X.; Alivisatos, A. P. Interaction potentials of anisotropic nanocrystals from the trajectory sampling of particle motion using in situ liquid phase transmission electron microscopy. *ACS Cent. Sci.* **2015**, *1*, 33–39.
- (30) Tan, S. F.; Raj, S.; Bisht, G.; Annadata, H. V.; Nijhuis, C. A.; Král, P.; Mirsaidov, U. Nanoparticle interactions guided by shape-dependent hydrophobic forces. *Adv. Mater.* **2018**, *30*, 1707077.
- (31) Ou, Z.; Wang, Z.; Luo, B.; Luijten, E.; Chen, Q. Kinetic pathways of crystallization at the nanoscale. *Nat. Mater.* **2020**, *19*, 450–455.
- (32) Chen, W.; Guo, J.; Zhao, Q.; Gopalan, P.; Fafarman, A. T.; Keller, A.; Zhang, M.; Wu, Y.; Murray, C. B.; Kagan, C. R. Designing strong optical absorbers via continuous tuning of interparticle interaction in colloidal gold nanocrystal assemblies. *ACS Nano* **2019**, *13*, 7493–7501.
- (33) Chen, W.; Tymchenko, M.; Gopalan, P.; Ye, X.; Wu, Y.; Zhang, M.; Murray, C. B.; Alu, A.; Kagan, C. R. Large-area nanoimprinted colloidal Au nanocrystal-based nanoantennas for ultrathin polarizing plasmonic metasurfaces. *Nano Lett.* **2015**, *15*, 5254–5260.
- (34) Jiang, N.; Zhuo, X.; Wang, J. Active plasmonics: Principles, structures, and applications. *Chem. Rev.* **2018**, *118*, 3054–3099.
- (35) Israelachvili, J. N. Chapter 14 - Electrostatic Forces between Surfaces in Liquids. In *Intermolecular and Surface Forces*, 3rd ed.; Israelachvili, J. N., Ed.; Academic Press: San Diego, 2011; pp 291–340.
- (36) Kim, J.; Song, X.; Ji, F.; Luo, B.; Ice, N. F.; Liu, Q.; Zhang, Q.; Chen, Q. Polymorphic assembly from beveled gold triangular nanoprisms. *Nano Lett.* **2017**, *17*, 3270–3275.
- (37) Walker, D. A.; Leitsch, E. K.; Nap, R. J.; Szeleifer, I.; Grzybowski, B. A. Geometric curvature controls the chemical patchiness and self-assembly of nanoparticles. *Nat. Nanotechnol.* **2013**, *8*, 676–681.
- (38) Gerbode, S. J.; Lee, S. H.; Liddell, C. M.; Cohen, I. Restricted dislocation motion in crystals of colloidal dimer particles. *Phys. Rev. Lett.* **2008**, *101*, No. 058302.
- (39) Sun, L.; Lin, H.; Park, D. J.; Bourgeois, M. R.; Ross, M. B.; Ku, J. C.; Schatz, G. C.; Mirkin, C. A. Polarization-dependent optical response in anisotropic nanoparticle–DNA superlattices. *Nano Lett.* **2017**, *17*, 2313–2318.
- (40) Savage, J. R.; Blair, D. W.; Levine, A. J.; Guyer, R. A.; Dinsmore, A. D. Imaging the sublimation dynamics of colloidal crystallites. *Science* **2006**, *314*, 795–798.
- (41) Chen, W.; Liu, W.; Jiang, Y.; Zhang, M.; Song, N.; Greybush, N. J.; Guo, J.; Estep, A. K.; Turner, K. T.; Agarwal, R.; Kagan, C. R. Ultrasensitive, mechanically responsive optical metasurfaces via strain amplification. *ACS Nano* **2018**, *12*, 10683–10692.
- (42) Kravets, V. G.; Kabashin, A. V.; Barnes, W. L.; Grigorenko, A. N. Plasmonic surface lattice resonances: A review of properties and applications. *Chem. Rev.* **2018**, *118*, 5912–5951.
- (43) Kuczynski, G. C. Study of the sintering of glass. *J. Appl. Phys.* **1949**, *20*, 1160–1163.
- (44) Niu, K.-Y.; Liao, H.-G.; Zheng, H. Visualization of the coalescence of Bismuth nanoparticles. *Microsc. Microanal.* **2014**, *20*, 416–424.
- (45) Mohamed-Kassim, Z.; Longmire, E. K. Drop coalescence through a liquid/liquid interface. *Phys. Fluids* **2004**, *16*, 2170–2181.
- (46) Aarts, D. G. A. L.; Schmidt, M.; Lekkerkerker, H. N. W. Direct visual observation of thermal capillary waves. *Science* **2004**, *304*, 847–850.
- (47) Chen, R.; Zhu, K.; Gan, Q.; Yu, Y.; Zhang, T.; Liu, X.; Ye, M.; Yin, Y. Interfacial solar heating by self-assembled Fe₃O₄@C film for steam generation. *Mater. Chem. Front.* **2017**, *1*, 2620–2626.
- (48) Li, B.; Wen, X.; Li, R.; Wang, Z.; Clem, P. G.; Fan, H. Stress-induced phase transformation and optical coupling of silver nanoparticle superlattices into mechanically stable nanowires. *Nat. Commun.* **2014**, *5*, 4179.